Investigation of novel carboxymethyl chitosan-based bioinks for 3D bioprinting of neural tissues

IOP Publishing Biomed. Mater. 20 (2025) 035036 https://doi.org/10.1088/1748-605X/add6f9

Biomedical Materials

OPEN ACCESS

RECEIVED
9 January 2025

REVISED
17 April 2025

ACCEPTED FOR PUBLICATION
9 May 2025

PUBLISHED
19 May 2025

PAPER

Investigation of novel carboxymethyl chitosan-based bioinks for 3D bioprinting of neural tissues

Amanda C Juraski[1,2,4], **Victor A da Silva**[2,4], **Ruchi Sharma**[2], **Adriano R Azzoni**[1] and **Stephanie M Willerth**[2,3,*]

[1] Departamento de Engenharia Química, Escola Politécnica, Universidade de São Paulo, São Paulo, Brazil
[2] Department of Mechanical Engineering & Division of Medical Sciences, University of Victoria, Victoria, Canada
[3] School of Biomedical Engineering, University of British Columbia, Vancouver, British Columbia, Canada
[4] co-first authors.
[*] Author to whom any correspondence should be addressed.

E-mail: willerth@uvic.ca

Keywords: 3D bioprinting, bioink, carboxymethyl chitosan, alginate, Fibrin, neural tissue engineering

Supplementary material for this article is available online

Abstract

The formulation of bioinks is critical for successful 3D bioprinting. It influences printability, stability, and cell behavior. One of the main demands in 3D bioprinting is the development of bioink formulations that can balance long-term cell viability and compositional similarities to the extracellular matrix (ECM) with rheological properties for 3D printing. To address this challenge, this study tested new bioinks using carboxymethyl chitosan (N,O-CMCS or O-CMCS), alginate, and fibrin, which are promising biomaterials due to their biocompatibility and likeness to the ECM. 3D bioprinting of neural tissues comes with additional challenges because neural cells are highly sensitive to environmental conditions. Therefore, we optimized our bioink formulations for the 3D bioprinting of neural progenitor cells derived from human induced pluripotent stem cells (hiPSC-NPC). Here we report a neural tissue constructed 3D bioprinted with a hiPSC-NPC-laden 1% N,O-CMCS, 1% alginate, and 20 mg ml^{-1} fibrin. This formulation exhibited uniform consistency and minimal extrusion force fluctuations (approximately 8 KPa), indicating homogeneity and optimal printability using an extrusion-based bioprinter. In contrast, O-CMCS formulations did not support neural tissue differentiation while higher concentrations of N,O-CMCS or alginate (3% w/v) resulted in increased viscosity and poorly defined scaffolds. The optimized bioink demonstrated significant water retention, swelling up to 15 times its original weight without losing structural integrity, thus providing a conducive environment for cell culture. Live/dead staining revealed over 60% cell viability over 30 d, underscoring its suitability for long-term cell applications. Immunocytochemistry confirmed that the optimized N,O-CMCS-based bioink effectively guided cells toward further differentiation into neurons and astrocytes, thus forming a 3D bioprinted construct that is able to replicate different neural cell types found in the neural tissue. The optimized bioink described in this study lays the groundwork for future works that will focus on detailing how different CMCS groups affect tissue maturation and functionality in 3D bioprinted constructs that can potentially be used for future neural tissue modeling and drug screening.

1. Introduction

Three-dimensional (3D) bioprinting has emerged as a transformative technology in tissue engineering and regenerative medicine, offering the promise of creating complex, functional tissue structures with remarkable precision [1]. This innovative technique enables the fabrication of intricate tissue models that closely mimic the natural environment of cells, surpassing the limitations of traditional 2D cultures in terms of replicating cell–cell interactions and tissue complexity [2, 3]. These advanced

models hold tremendous potential for studying tissue development, disease mechanisms, drug screening, and transplantation therapies, making them crucial for advancing tissue engineering strategies [4, 5].

A key aspect for the success of 3D bioprinting is the development of bioinks—specialized materials that encapsulate cells and support their organized growth within printed structures [3]. Ideal bioinks should emulate the physical, chemical, and rheological properties of native tissues to ensure optimal cell function and survival [6]. That poses a challenge for 3D bioprinting because soft hydrogels that support cell viability usually display rheological properties unfit for 3D bioprinting, and stiff hydrogels that are easily printed affect cell viability and differentiation [7]. Bioink formulation is therefore decisive for ensuring long-term cell viability and printability [8]. This is especially significant for 3D bioprinting neural tissues because neural cells are highly sensitive to environmental conditions [7, 9]. An optimized bioink should be able to sustain long-term cell viability, allow tissue maturation, and display the rheological properties compatible with 3D bioprinting. Developing optimized bioinks with known formulations is crucial for future translation of 3D bioprinted constructs into clinical applications [6, 8]. The interest in developing 3D bioprinted neural tissue constructs is that 3D models offer a more accurate *in vitro* replication of the natural tissue's architecture, including cell arrangement, extracellular matrix (ECM) disposition, therefore offering a pathway towards a better *in vitro* model of real biological conditions [10, 11]. When compared to other 3D systems, such as brain organoids, 3D bioprinted neural tissues usually offer better cell distribution and ECM replication, leading to overall enhanced tissue cell maturation and tissue organization. 3D bioprinted constructs also enable scalable production of neural tissue constructs. Organoids, on the other hand, form through self-organization and display high variability in important features, such as size, shape, cellular composition and distribution, making it harder to achieve consistent reproducibility and scalability [12, 13].

Among the array of biomaterials explored for bioinks, natural-sourced hydrogels such as carboxymethyl chitosan (CMCS), alginate, and fibrin have garnered considerable attention due to their biocompatibility, compositional similarities to the ECM, and functional benefits in supporting cell viability and differentiation [5, 14–16]. Chitosan is a naturally sourced amino-polysaccharide with physicochemical and biological properties such as non-toxicity, biodegradability, and biocompatibility. It has glucosamine and *N*-acetyl glucosamine units linked by β (1–4) glycosidic bonds formed in the *N*-deacetylation process of chitin [17]. However, chitosan is insoluble in water at neutral pH, which severely hinders its applicability in bioinks. Carboxymethyl chitosan (CMCS) is a water-soluble derivative of chitosan obtained through the substitution of chitosan's hydroxyl ($-OH$) and amino ($-NH_2$) groups for carboxymethyl groups. When substitution happens only at the $-OH$ groups, O-CMCS is formed. Likewise, when substitution happens at $-OH$ and $-NH_2$ groups, N,O-CMCS is formed. CMCS offers enhanced biocompatibility and biodegradability when compared to its insoluble parent material. CMCS has already been explored as a bioink component for 3D bioprinting neural tissues, with sustained human neural stem cells survival due to the porosity and water permeability offered by CMCS [5]. Moreover, whilst both N,O-CMCS and O-CMCS exhibit improved water retention and biocompatibility when compared to their parent polysaccharide, making them promising candidates for bioink formulations, they also display different physicochemical properties due to the two types of substituted groups during carboxymethylation. Therefore, it is necessary to investigate which CMCS form would be most appropriate for bioinks applied to neural tissue engineering [16, 18–21]. However, CMCS alone lacks the rheological properties and crosslinking motifs necessary for 3D printing applications. Alginate, a polysaccharide derived from seaweed, on the other hand, is known for its mild gelation properties and excellent biocompatibility. It possesses mannuronic and guluronic acid monomers that can easily be crosslinked by Ca^{2+}. When combined, CMCS and alginate can easily be crosslinked together by calcium ions into a stable and interpenetrative network with improved rheology and antibacterial properties [22–24]. CMCS and alginate hydrogels have been combined as a bioink for bone tissue engineering [25], enamel regeneration [26], and the biofabrication of neural mini-tissues [5], but there is still the need to optimize the hydrogels' concentrations for 3D printing of neural tissues. Moreover, CMCS can be synthesized in different forms depending on the chitosan groups substituted by carboxyl groups, which can affect the bioink's physiochemical and biological properties. Although both CMCS and alginate are biocompatible polysaccharides, they lack specialized molecular interactions to promote mammalian cells attachment and penetration, which are needed for proper stem cell differentiation and tissue formation. Fibrin, a protein involved in blood clotting and tissue repair, closely resembles the native ECM, providing essential support for cell attachment, migration, and tissue remodeling [27]. Fibrin-based bioinks have demonstrated significant potential in bioprinting various tissue models, including neural tissues [2, 28].

The technique employed to obtain 3D bioprinted neural tissues can also affect cell viability. Extrusion-based bioprinting is a popular method for 3D bioprinting due to its versatility and ability to produce bioprinted constructs with high cell density [7, 29, 30]. The extrusion method uses a layer-by-layer deposition of the bioink following a pre-designed layout. That allows the combination of different materials in the same printing process, with different types of hydrogels and cells to be loaded in the same bioink formulation, consequently leading to a better replication of the ECM's composition and complexity [31, 32]. Moreover, when compared to other bioprinting methods such as laser-based and inkjet bioprinting, extrusion-based 3D bioprinting offer less sheer stress and is more adaptable, cost-effective and scalable, making it a valuable asset for translational 3D bioprinting [7, 8].

The aim of this study was the development and characterization of novel bioinks formulated with N,O-CMCS and O-CMCS, combined with alginate and fibrin, for 3D bioprinting neural tissues using neural progenitor cells derived from human induced pluripotent stem cells (hiPSC-NPCs) using an extrusion-based commercial 3D bioprinter. We present the characterization of rheological properties, printability, physicochemical characteristics, and biological performance of selected optimized formulations. Using a 1% N,O-CMCS 1% alginate and 20 mg ml^{-1} fibrin bioink we were able to fabricate a 3D bioprinted neural tissue with different cell types found in the human neural tissue. Overall, we believe that this study can offer new insights as to how the physiochemical interactions between bioink components affect its biological response regarding cell viability and differentiation. The neural tissues 3D bioprinted using the selected formulation could be applied to future tissue engineering and drug screening applications.

2. Material and methods

2.1. Materials

Chitosan (C3646 lot SLBW1036, poly β-1,4-D-glucosamine derived from shrimp shells, degree of deacetylation $\geqslant$ 75%, molecular weight 800 kDa, viscosity 16 cps) [33–35], monochloroacetic acid (402923), 2-propanol (278475), low viscosity alginic acid sodium salt (180947, M/G:1.56, molecular weight 120–190 kDa) [36, 37], calcium chloride (C1016), thrombin (T7009), β-glycerophosphate (G9422), poly-L-ornithine (P4957), laminin (L2020) and Triton X-100 (T8787) were purchased from Sigma-Aldrich. Fibrinogen (341578) was purchased from EMD Millipore. STEMDiff Neural Progenitor Medium (05834), STEMDiff Neural Progenitor supplement A (05836), STEMdiff Neural Progenitor supplement B (05837) and STEMdiff Neural Progenitor freezing medium (05838) were purchased from Stemcell Technologies. Live/Dead Viability/Cytotoxicity Kit (L3224), paraformaldehyde (J19943-K2), and DAPI (D1306) were purchased from ThermoFisher Scientific. Dulbecco's phosphate-buffered saline (D-PBS) (30–2200) was purchased from ATCC. Normal goat serum (NGS) (ab7481), βIII tubulin (ab231084), glial fibrillary acidic protein (GFAP) (ab68428), Alexa 488 fluorescent secondary antibody (ab15011) and Alexa 568 fluorescent secondary antibody (ab175476) were purchased from Abcam. Paired Box 6 (PAX6) (42–6600) was purchased from Invitrogen. Purchased materials were used as received. All other reagents used were at least, regent grade.

2.2. Preparation of bioinks

First, chitosan was carboxymethylated with monochloroacetic acid/2-propanol (1:1 w/w) following previously described methods to prepare N,O-CMCS and O-CMCS [38, 39]. After neutralization and purification, the product was analyzed with attenuated total reflection using Fourier transform infrared spectroscopy (FTIR) to ensure substitution of carboxymethyl groups at amino and/or hydroxyl groups of the chitosan. The substitution degree for N,O-CMCS and O-CMCS was determined by potentiometric titration. The CMCS/alginate/fibrin bioinks were prepared based on a previously established protocol [15]. Briefly, either N,O-CMCS or O-CMCS was prepared at 3% w/v by dissolving in distilled water and sterilized by autoclaving. Sodium alginate solution was prepared at 3% w/v by reconstituting in distilled water and sterilized using 0.2 μm syringe filter. The final concentrations of CMCS and alginate in the bioink was either 3% or 1%. Fibrinogen was prepared at a concentration of approximately 50 mg ml^{-1} in tris-buffered saline (TBS) solution and sterilized using 0.22 μm syringe filters. The final concentration for fibrinogen was adjusted to either 10 or 20 mg ml^{-1} in the bioinks. Six different formulations were tested out, varying CMCS form or hydrogel fraction. Bioink formulations are described on table 1. The crosslinking solution combined calcium chloride ($CaCl_2$), thrombin, and chitosan. $CaCl_2$ was prepared at a concentration of 20 mg ml^{-1} in TBS. Thrombin was reconstituted at a concentration of 1000 U ml^{-1} in sterile TBS. The final concentration of thrombin was 1.7 U ml^{-1} in the crosslinker. Chitosan was prepared at a concentration of 25 mg ml^{-1} using 1% acetic acid and its pH was adjusted to 7.4 using β-glycerophosphate (β-GP). The final concentration of chitosan in the crosslinker was 0.075% w/v. The crosslinking solution was sterilized by filtering using 0.22 μm syringe filters.

2.3. 3D printing of CMCS/alginate/fibrin biomaterial inks

The hydrogel solution was loaded into 3 ml plastic cartridges (CSC010300102, CELLINK) and attached to dispensing nozzles (NZ4220005001, CELLINK) for precise printing using the BioX 3D printer (D16110020717, CELLINK) [40]. The 3D printing design was a grid structure with 40% rectilinear infill and 1 mm × 1 mm layers. Pressure parameters ranged from 3 KPa to 20 KPa depending on the bioink formulation, and bioprinting speed was 10 mm s^{-1} . Constructs were printed into sterile agarose (1% w/v) support baths in cell culture plates. After printing, enough crosslinker to submerge the constructs was added to the edges of the well using a micropipette, and incubated for 3 min. Afterwards, the cell-free constructs were removed from the agarose bath, washed with sterile PBS to remove any residual agarose, transferred into a clean cell culture plate filled with fresh PBS and incubated at 4 °C until characterizations.

2.4. Printability

For each formulation, cell-free constructs were imaged using a cellphone camera (Redmi Note 9 S, Xiaomi) with 2X augmentation immediately after crosslinking and removal of the agarose support bath. Constructs were imaged immediately after the printing of two layers [1]. Pictures were taken at a distance of 6 cm and external light was used to achieve enough contrast. The images were processed using Fiji image processing software (ImageJ, GNU General Public License) where the pore area (A) and perimeter (L) of each pore in the scaffold was determined for each bioink formulation. The printability of the bioinks was determined using equation (1), where L is the perimeter of the pore, A is the area of the pore, and Pr is printability which characterizes the structural integrity of the material. A bioink with ideal printability ($Pr = 1$), would possess clear morphology with a smooth surface and constant 3D width which results in regular grids and square pores in the printed construct. In the case of under gelation ($Pr < 1$), a slurry filament is printed where the upper and lower layers of the scaffold fuse and subsequently cause pores to develop a more circular form. In the case of over-gelation ($Pr > 1$), layers do not fuse into a uniform construct [20].

$$\mathrm{Pr} = {}^{L^2}/_{16 * A}. \tag{1}$$

2.5. Rheological properties

The rheological properties of the hydrogels were measured on crosslinked cell-free constructs 24 h after printing. The analyses were performed using a rheometer (MCR302, Anton Paar) equipped with sandblasted parallel-plate fixtures (PP25/S, 3997, Anton Paar) of diameter 25 mm with a gap width of 1 mm [41]. Each construct was loaded onto the plate (25 ± 2 °C) to determine the shear moduli. Squared-shaped constructs were loaded on the rheometer to determine the modulus of the 3D bioprinted constructs. The frequency sweep was conducted from 0.1 to 100 rad s^{-1} at a 0.5% strain to measure frequency-dependent storage (G') and loss (G'') moduli. The viscosity was measured at shear rates from 0.01 to 90 s^{-1}. Data was collected using Anton Paar RheoCompass software.

2.6. Physicochemical characterization of bioink

The FTIR spectroscopy of each bioink component and selected formulations was obtained from ground powder of lyophilized samples, using the attenuated total reflectance accessory (FTIR-ATR, Spectrum Two, PerkinElmer).

The swelling ratio of crosslinked constructs using the selected formulations was measured by weighing the swollen printed samples after incubation in PBS. After printing, the samples were slightly bloated and weighted (Wi), and then incubated in PBS at 37 °C for 24 h. Then, the samples were removed from the PBS, and the final wet weight of the samples was determined (Wf). The swelling ratio of the constructs was calculated by equation (2). Three samples were recorded in three independent replicates for each of the selected formulations

$$\text{Swelling ratio} = (Wf - Wi)\,/Wf. \tag{2}$$

2.7. Culture and expansion of hiPSC-NPCs

Cell culture and expansion of hiPSC-NPCs followed a previously described method [42] using a 1-DL-01 (male) cell line from WiCell under the approval of University of Victoria's Human Ethic Committee protocol number: 12–187. hiPSC-NPCs were cultured and expanded in 6 well-plates coated with poly-L-ornithine (PLO) and laminin. Cells were cultured using the STEMDiff Neural Progenitor Medium (NPM) supplemented with 1x STEMDiff Neural Progenitor supplement A and 1x STEMdiff Neural Progenitor supplement B. Media was changed every other day until reaching 80% confluency at 37 °C in 5% CO_2. Cryopreservation of hiPSC-NPCs was carried out at a cell density of 1 × 10^6 cells ml^{-1} in STEMdiff Neural Progenitor freezing medium.

2.8. Direct contact assay

The direct test was performed according to ISO 10 993–5:2009 to analyze cell morphology and viability in direct contact with the selected formulations. Cells were incubated for 3 d before the contact test. For the direct contact assay, cell-free 3D printed constructs were obtained under sterile conditions following the procedures described in section 2.3. Immediately after printing and crosslinking they were gently placed on top of the cell layers, using a 1 cm^2

piece of each hydrogel and 1 ml of medium per well in a 24-well plate. Viability testing was conducted on days 1, 3 and 7. Tests were conducted in triplicate, with filter paper as the negative control (NEG, known to be non-cytotoxic) and latex as the positive control (POS, known to be cytotoxic). The morphological analysis was carried out using a microscope (DMI3000B, Leica Microsystems), and Live/Dead Viability/Cytotoxicity Kit was used to assess cell viability. For each group, it was selected as a result the image that best represented the overall counting result. Cell viability (expressed in %) was calculated as the ratio between the green stained area (live cells) and the total stained area (live cells and dead cells) of the images using the Fiji software ($n = 6$ different spots into three different constructs) [43]. To maintain consistency in brightness and contrast, all images were processed using Fiji. Adjustments were applied uniformly by referencing the grayscale histogram, ensuring that intensity distributions remained comparable across all samples. This method helped prevent over- or under-enhancement while preserving data integrity. Finally, individual fluorescence channels were merged to generate composite images, allowing for a clearer representation of colocalization and spatial distribution of the observed structures [44].

2.9. 3D bioprinting CMCS/alginate/fibrin bioinks with hiPSC-NPCs

hiPSC-NPCs were thawed and then resuspended in warm DMEM and centrifuged at 300 g for 5 min. The supernatant was removed, and the hiPSC-NPCs were resuspended at a concentration of 2×10^6 cells ml^{-1} in the CMCS/alginate/fibrin solution, forming the bioink. 3D bioprinting followed the same procedure as described previously. All procedures were performed under sterile conditions. Constructs were then moved into PLO/laminin coated plates and cultured in the same way as hiPSC-NPCs.

2.10. Culture of bioprinted constructs

From days 0–30, the bioprinted constructs were cultured in STEMDiff NPM supplemented with 1x STEMDiff Neural Progenitor supplement A and 1x STEMdiff Neural Progenitor supplement B. Media changes were carried out every other day by replacing half of the total volume with fresh media. The bioprinted constructs were maintained at 37 °C in 5% CO_2.

2.11. 3D bioprinted constructs live/dead cell viability assay

The viability of cells inside the constructs was analyzed using the Live/Dead Viability/Cytotoxicity Kit. Viability testing was conducted on days 7, 15, 25, and 30. First, the media was removed from the constructs, and each construct was washed with D-PBS. The staining solution consisted of 2 μM calcein-AM, to stain live cells, and 4 μM ethidium homodimer-1, to stain dead cells, both in D-PBS. Constructs were incubated in the staining solution for 45 min at 37 °C and 5% CO2 in the dark. After incubation, the constructs were imaged using an inverted microscope. Live cells were imaged using 475 nm (green light), and dead cells were imaged using 510 nm (red light). Images were acquired at three different spots for each construct. Using Fiji image processing software, cells were manually counted in the channels of green (live cells) and red (dead cells). Cell viability (%) was calculated as the ratio of the number of green (live) cells to the total number of cells (sum of green and red cells). Tests were conducted in triplicate, resulting in a total of 9 images analyzed for each group.

2.12. Immunocytochemistry (ICC)

Constructs were fixed for 30 min in 4% paraformaldehyde (PFA) and washed three times with PBS. Membrane permeabilization was performed using 0.4% Triton X-100 in PBS at 4 °C for 45 min. After washing with PBS, 5% NGS in PBS was added at 4 °C for 2 h to block non-specific binding. Following another PBS wash, cells were incubated overnight with gentle shaking at 4 °C with primary antibodies. These included 1 μg ml^{-1} βIII tubulin (TUJ1) as a neuronal marker, 0.5 μg ml^{-1} GFAP as a glial astrocytic marker or 2.5 μg ml^{-1} PAX6 as a transcription factor marker for neural progenitor cells. The primary antibodies were diluted in a solution containing 5% NGS in 0.1 M Phosphate Buffer (PB). On the following day, constructs were washed three times with PBS and then incubated with 1:600 Alexa 488 fluorescent secondary antibody and 1:600 Alexa 568 fluorescent secondary antibody diluted in 0.3% Triton X-100 in 0.1 M PB for 4 h at room temperature. Following additional PB washes, constructs were incubated with 300 nM DAPI for 5 min and then washed three times before imaging with an inverted microscope (TS100F, Nikon Instruments). The control of autofluorescence was accounted for by capturing images in a control channel 3D bioprinted scaffolds without antibody staining (background fluorescence) and then subtracting that intensity from the antibody channel signal. Analyses were conducted in triplicate, resulting in a total of 9 images analyzed for each group.

2.13. Statistical analysis

All data were expressed as mean ± standard error ($n = 3$ for all experiments). Statistical analysis printability, for viscosity, storage modulus, loss modulus, and ICC were carried out using one-way ANOVA analysis of variance with a Tukey post-hoc analysis, with 95% confidence.

Statistical analysis for swelling degree and live/dead assay was carried out using an unpaired

t-test for parametric data and Mann–Whitney for non-parametric data. A value of $p < 0.05$ was considered statistically significant. All statistical analysis was carried out using the GraphPad Prism 8 statistics software.

3. Results and discussion

3.1. Preparation of bioinks and 3D bioprinting of hiPSC-NPCs

The overall method for each CMCS/alginate/fibrin bioink preparation is illustrated in figure 1. Chitosan, the precursor polysaccharide of CMCS, is only soluble in acidic pHs (pH < 6), which limits its biomedical applicability in physiological conditions (pH 7.4) [22]. To overcome this, the synthesis of chitosan derivatives such as CMCS has been employed. CMCS is an amphoteric polyelectrolyte derived from the carboxylation of chitosan, and therefore has carboxyl, amino and hydroxyl groups available on each polymer chain, making it soluble in water in neutral pH. When CMCS synthesis is carried out under heat (>65 °C), carboxymethyl groups replace both hydroxyl and amino groups, forming N,O-CMCS [45]. On the other hand, when synthesis is carried out at room temperature, the reaction favors the replacement of hydroxyl groups, forming O-CMCS [22]. Potentiometric titration indicated a degree of substitution of 0.49 and 0.44 for N,O-CMCS and O-CMCS, respectively. After CMCS synthesis, the hydrogels were mixed with alginate and fibrin solutions, as described on table 1, resulting in different bioinks used for bioprinting the hiPSC-NPC-laden constructs. These biomaterials were chosen for their biocompatibility with neuronal cells, specifically with hiPSC-NPCs, and successful printability with extrusion-based bioprinters [20, 26, 40]. However, to the best of out knowledge there had not been a previous study that optimizes these components into a bioink aimed at 3D bioprinting of neural tissues.

3.2. Printability

Figures 2(a)–(f) shows the 3D printed lattice structures with 40% rectilinear infill and 1 mm × 1 mm layers of bioink. Printability of each bioink (B1—B6) was evaluated by its uniform ejection and shape retention, with minimal variations in extrusion force (varying from 8 kPa to 40 kPa) required for printing and calculated using equation (1). Figure 2(g) shows an example of how printability values and shape fidelity are correlated. CMCS form affected printability significantly, but there was no statistical difference from hydrogel fraction (figure 2(h)). N,O-CMCS based bioinks (B1 to B3) had printability values of 0.96 ± 0.01, 0.98 ± 0.01 and 0.95 ± 0.01, respectively. O-CMCS based bioinks (B4 to B6) had printability values of 0.93 ± 0.01, 0.94 ± 0.01 and 0.93 ± 0.01, respectively. While all bioinks showed printability values within the acceptable range (0.9–1.0) [20], B1 and B3 constructs' layers were not uniform. B2 constructs on the other hand, required low extrusion force (8 kPa), and presented uniform layers and shape fidelity. Likewise, B4 and B6 constructs required high extrusion forces (40 kPa), and lacked extrusion uniformity and shape fidelity, whilst B5 constructs were printed with a lower extrusion forced (20 kPa) and presented both layer uniformity and shape fidelity. Shape fidelity is an important characteristic for 3D printed constructs because it affects cell viability and differentiation. A lack of layer uniformity and shape fidelity will impact cell distribution and settling during 3D bioprinting and impede proper oxygen and nutrient delivery [23].

3.3. Rheological properties

Rheological properties play key roles in successful bioprinting, cell viability, and differentiation. Here, the viscosity and frequency sweeps of N,O-CMCS (B1 to B3) and O-CMCS (B4 to B6) based bioinks were measured using an Anton Paar Rheometer to test how these formulations and hydrogel volumes affected the viscoelastic properties of the 3D printed constructs (figure 3).

The viscosity was analyzed by regression analysis using the Carreau–Yasuda method with shear rate from 0.01 to 90 s^{-1}. Figure 3(a) shows that, while viscosity was dependent on shear rate, all formulations displayed shear-thinning behavior. This is an important bioink property because it enables continuous hydrogel flow during printing and protects the cells from strenuous shear forces [41]. G' and G'' are values associated with the viscous and elastic aspects of a material, respectively. Figure 3(b) shows how the tan delta value (tanδ) changes over a frequency sweep. The tanδ value represents the ratio between the loss modulus (G'') and the storage modulus (G'), and reflects the balance between the viscosity, elasticity, and energy storage properties of a material [46]. For the entire frequency sweep, the tanδ of all formulations was consistently below 1, signifying that the constructs were predominantly elastic with solid-like behavior. This is a desirable feature for hydrogels applied to bioprinting because it guarantees constructs will retain integrity and shape fidelity during printing. Moreover, figure 3(c) shows that when shear stress is equal to shear strain (shear rate = 1), the B2 formulation had the highest viscosity at 269.130 Pa.s. Statistical analysis did not find any significant effect of either CMCS formulation or hydrogel fraction on viscosity. A fibrin-based bioink that used the same crosslinking solution had similar solid-like behavior, with viscosity also decreasing as shear stress increased [41, 47].

Figures 3(d) and (e) show that at the beginning of the frequency sweep (1 rad s^{-1}), the B2 formulation had the highest G' (823.6 kPa') and G'' (133.2 kPa).

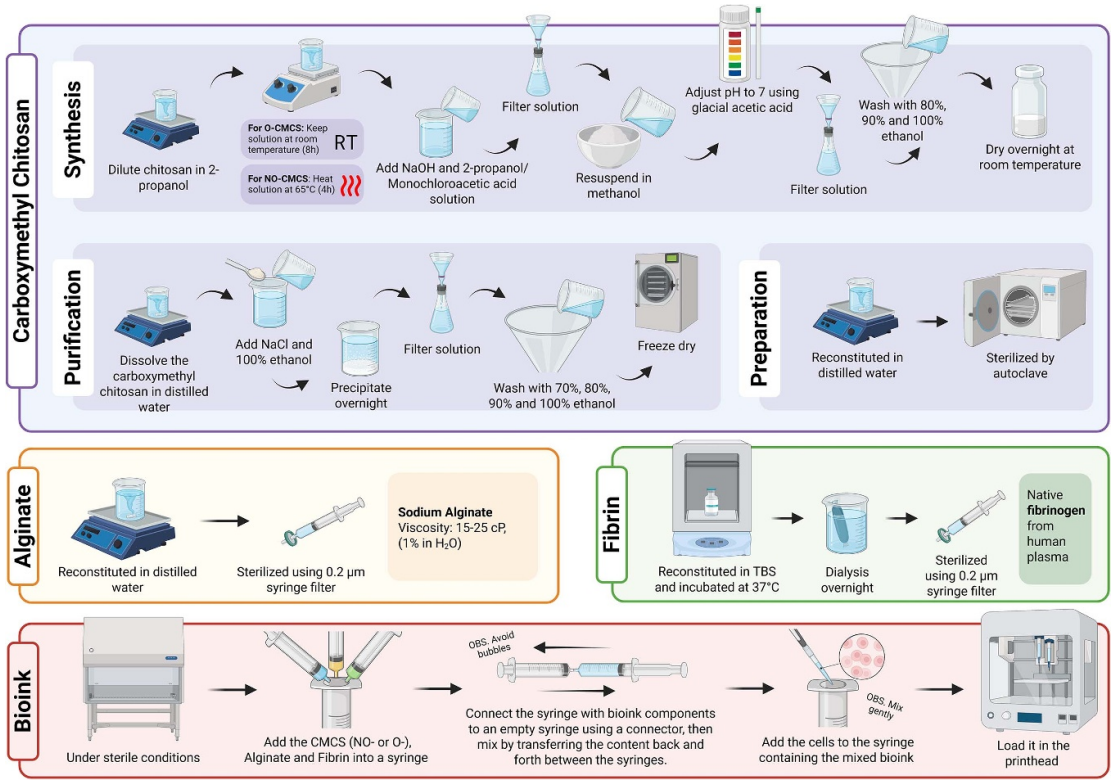

Figure 1. Schematic of the main steps in preparation of CMCS/alginate/fibrin bioink using hiPSC-NPCs for neural tissue models. Bioink started with the synthesis of O-CMCS and N,O-CMCS, followed by reconstitution of CMCS and alginate (3% w/v) in distilled water. Fibrin solution was prepared by reconstitution in TBS. To form the bioink, the hydrogels were mixed with hiPSC-NPCs under sterile conditions. The bioink syringe was then connected to the BioX printheads and 3D constructs were obtained through extrusion printing into an agarose bath, and crosslinked by addition of a $CaCl_2$/thrombin/chitosan solution.

Table 1. Hydrogels and concentrations used for bioink formulations.

Bioink	CMCS form	CMCS concentration	Alginate concentration	Fibrin concentration
B1	N,O-CMCS	1% (w/v)	1% (w/v)	10 mg ml^{-1}
B2				20 mg ml^{-1}
B3		3% (w/v)	3% (w/v)	20 mg ml^{-1}
B4	O-CMCS	1% (w/v)	1% (w/v)	10 mg ml^{-1}
B5				20 mg ml^{-1}
B6		3% (w/v)	3% (w/v)	20 mg ml^{-1}

Here, statistical analysis showed that while formulation and hydrogel fraction did not influence the storage modulus (G'), it did affect the loss modulus (G''). The significant difference in G'' value between B2 and B6 indicated that the B2 formulation has a solid-like behavior, while the B6 formulation has a more liquid-like behavior. This correlates to the improved shaped fidelity in B2 constructs when compared to B6 constructs. The higher concentrations of O-CMCS and alginate in the B6 formulation led to a lower loss modulus, likely due to O-CMCS poor mechanical properties and lower degree of crosslinking [26]. Nevertheless, for all constructs G' remained higher than G'', indicating that all ink formulations are able to store deformation energy in an elastic manner, regardless of formulation or hydrogel fraction [41]. Moreover, considering the printing, shape fidelity and rheological assessments, B2 and B5 formulations had the highest storage and loss modulus, and values compatible with other bioinks applied to neural tissue applications [1, 20, 23], likely due to the increased fibrin concentration, which can significantly impact cell survival [41, 48]. Therefore, the B2 and B5 formulations were selected for the following studies.

3.4. Physicochemical characterization of the bioink

3.4.1. FTIR

FTIR spectra were obtained to examine the physicochemical interactions between bioink components. The FTIR spectrum of each component and of the final 3D printed constructs are presented in figure 4. N,O-CMCS characteristic peaks (figure 4(a))

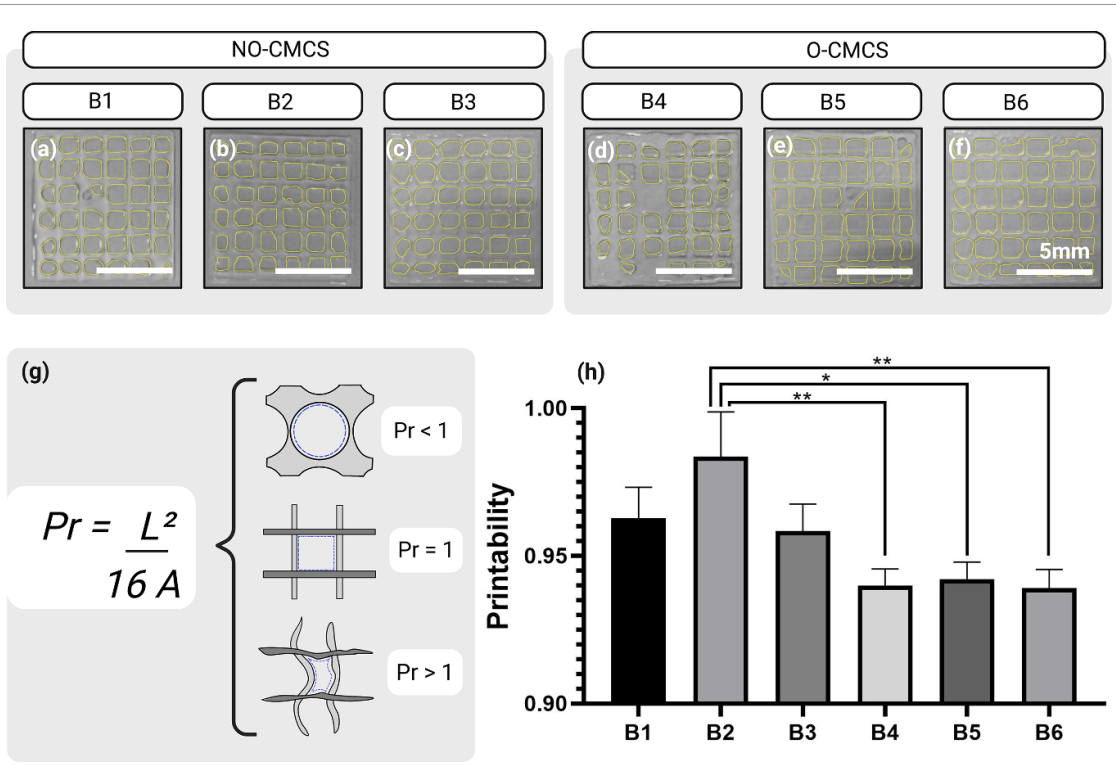

Figure 2. Printability evaluation. (a)–(f) 3D printed scaffolds using the different tested formulations (B1—B6). (g) Degree of gelation for filaments in a 3D printed construct. (h) Printability values for each tested formulation.

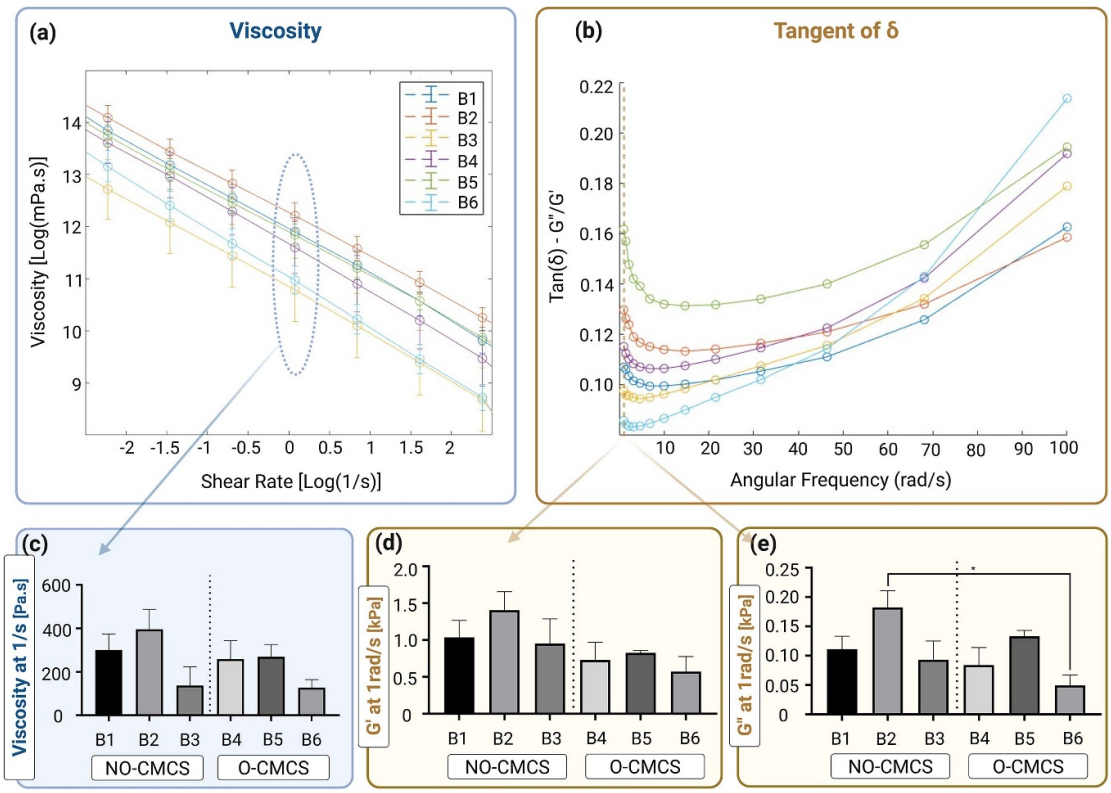

Figure 3. Rheological properties. (a) Viscosity versus shear rate curve of 3D printed constructs of each tested bioink. (b) Tanδ versus angular frequency of 3D printed constructs of each tested bioink. (c) Viscosity values at rest (shear rate = 1). (d) Storage modulus (G') values and (e) Loss modulus (G'') values. Data reported as mean ± standard error ($n = 3$). * means values are statistically different ($p < 0.05$) for one-way ANOVA analysis of variance with a Tukey post-hoc analysis.

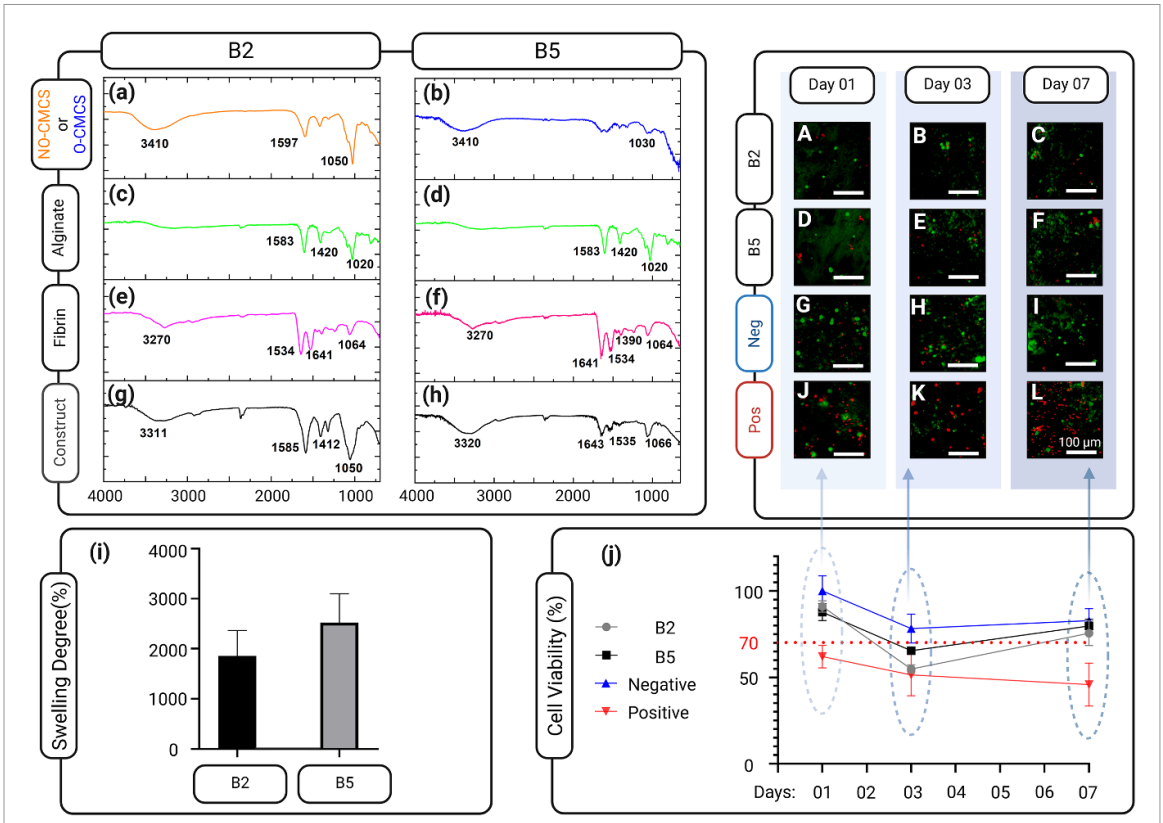

Figure 4. Physicochemical properties and direct contact test of selected bioink formulations. FTIR spectrum of (a) N,O-CMCS, (b) O-CMCS, (c) and (d) Alginate, (e) and (f) Fibrin, (g) 3D printed construct using B2 bioink formulation and (h) D printed construct using B5 bioink formulation. (i) Swelling study of 3D printed B2 and B5 samples. (j) hiPSC-NPC cell viability values from direct contact assay on B2 samples, B5 samples, negative control (filter paper) and positive control (latex) up to 7 d of cell culture. A-L) Confocal microscopy of hiPSC-NPC cells seeded on samples during direct contact assay (scale bar: 100 µm). Data reported as mean ± standard error ($n = 3$).

at 3410 cm^{-1} was attributed to O−H stretching of chitosan. The peaks at 1050 and 1597 cm^{-1} were assigned to the asymmetric and symmetric stretching of COO^- groups, indicating the successful carboxymethylation of the hydroxyl (−OH) and amine ($-NH_2$) groups of chitosan during N,O-CMCS synthesis. O-CMCS spectra (figure 4(b)) also presented the O–H stretching peak at 3410 cm^{-1} and the COO^- asymmetric stretching peak at 1030 cm^{-1}, indicating the carboxymethylation of only the −OH group during O-CMCS synthesis [22, 38, 39, 45]. Alginate's characteristic's peaks at 1583 and 1420 cm^{-1} (figures 4(c) and (d)) were attributed to the asymmetric and symmetric carboxyl polyanion, and the 1020 cm^{-1} peak was attributed to the C–OH vibration. Fibrin's peaks at 1641 and 1534 cm^{-1} (figures 4(e) and (f)) were associated with amide I and amide II groups, respectively [49]. The spectra of 3D printed constructs using the B2 bioink formulation (figure 4(g)) and the B5 bioink formulation (figure 4(h)) showed the same main peaks as their original bioink components. The absence of new peaks indicates that the hydrogels were bound via physical interactions, such as hydrogen bonds and electrostatic interactions [50]. During the bioink preparation process, the hydrogels were physically mixed together which induced electrostatic interaction between the components, as evidenced by the COO^- NH_2 peak shifts in B2 bioink spectra (figure 4(g)). The peak shifts from symmetric COO- groups in thee B2 construct (from 1597 to 1585 cm^{-1} and from 1420 to 1412 cm^{-1}) reinforces the presence of electrostatic interactions between N,O-CMCS and alginate, as well as the crosslinking of the carboxyl groups by the $CaCl_2$/thrombin/chitosan crosslinker solution [51]. These same changes were not observed in the B5 FTIR spectrum (figure 4(h)), indicating the lack of electrostatic interactions between O-CMCS and alginate and the lower crosslinking degree of the B5 constructs. The physical interaction between CMCS, alginate and fibrin also impacted the ink's rheological properties. Even though N,O-CMCS has a negative net charge at pH = 7.4, it still has protonated amino groups that can physically crosslink with negatively charged alginate and fibrin in addition of the ionic crosslinking with $CaCl_2$/thrombin/chitosan solution [26, 27]. This led to an increased value of viscosity, and storage and loss modulus for the B2 formulation (figures 3(c)–(e)). O-CMCS, on the other hand, while also negatively charged, has no protonated amino

groups at pH = 7.4. Therefore, O-CMCS interactions with alginate and fibrin (figure 4(h)) were likely mostly through hydrogen bonds [52].

3.4.2. Swelling degree

Ink water permeability was studied by measuring the constructs *in vitro* swelling degree (figure 4(i)). After 24 h of immersion in PBS (pH = 7.4), B2 and B5 constructs swelled 1600 ± 220% and 2530 ± 270%, respectively. The increased swelling in B5 bioink might be attributed to the lack of electrostatic interaction between the components. Even after ionic crosslinking with Ca^{2+}, it still has unbound carboxylic acid groups to interact with water molecules, as opposed to B2 bioink that has most of its protonated amino groups interacting with its own carboxylic groups, alginate, and fibrin [52, 53].

3.5. Bioink direct contact assay

The biocompatibility of B2 and B5 formulations were tested by direct contact assay before printing cell-laden constructs (figure 4(j)). Colocalization (yellow signal) was considered dead cells. The direct contact cell viability test showed that both formulations had significant cell death (over 25%) in the first three days of direct contact. B2 cell viability went from 91 ± 8% of cell viability on day 1–54 ± 5% of cell viability on day 3. The same pattern was observed for B5 constructs; from 88 ± 12% of cell viability on day 1–65 ± 4% of cell viability on day 3. However, afterwards both formulations displayed cell proliferation from day 3 to day 7. B2 and B5 samples reached 76 ± 16% and 80 ± 10% of cell viability on day 7, respectively. Confocal microscopy confirmed the presence of single cells in the first day post cell seeding, and the formation of cell aggregates as culture continued until day 7. (figures 4(A)–(I), supplemental figure S1).

3.6. 3D bioprinted constructs live/dead cell viability assay

After bioprinting the cell-laden samples, constructs were cultured in the same way as the hiPSC-NPCs. As cell viability decreased and increased significantly in the first seven days of culturing, cell viability for bioprinted samples was quantified on days 7, 15, 25 and 30 (figure 5(a)). On day 7, both formulations displayed similar cell viability, with the B2 formulation at 35 ± 10% and the B5 formulation at 48 ± 8%. However, by day 15, there was a significant difference in cell viability between the two formulations; the B2 showed cell proliferation and cell viability increased to 48 ± 10%, whereas the B5 formulation showed significant cell death and cell viability was reduced to 15 ± 3% (figure 5(b)). In the following days both groups had cell proliferation, but at different rates; by day 30, B2 samples reached 85 ± 6% of cell viability, whilst B5 constructs reached 35 ± 11% of cell viability. The difference in cell violability could be attributed to the presence of both physical and ionic crosslinking in the B2 constructs, as opposed to the B5 constructs that only had ionic crosslinking. With a tighter network, the N,O-CMCS-based bioink could have better retained the nutrients necessary for cell proliferation. An important observation is the decrease in cell viability after day 7 in both bioinks, reaching its lowest point on day 25, followed by a rapid increase by day 30. This phenomenon is commonly observed in extrusion-based bioprinting and may be attributed to mechanical stress and impact energies generated during extrusion through a conical needle [54]. Such mechanical forces can damage cell membranes, leading to reduced viability immediately after printing. Figure 5(i) shows the overlapping of a green and red signal, likely due to the presence of live and dead cells close to each other. The subsequent recovery in viability could be linked to the bioink's viscoelastic properties, which help mitigate the mechanical stresses experienced by cells, allowing for improved viability over time [55]. This finding highlights the importance of utilizing stem or progenitor cells in bioprinting applications, despite the initial challenges to viability [56]. The confocal images of the two selected bioinks over the 30 d are shown in figures 5(f)–(m). While both bioinks showed good rheological and printability properties, B5 was deemed not suitable for bioprinting due to its low biocompatibility. While O-CMCS is usually reported to be a safe biomaterial [57], in our study it showed a significant cytotoxic effect on hiPSC-NPCs. However, the N,O-CMCS-based B2 formulation displayed both the expected rheological and printability properties for a bioink, as well as a suitable cell viability for bioprinting applications [20].

3.7. ICC

An ICC analysis was performed as previously described to visualize whether the different bioink formulations affected the hiPSC-NPCs cell fate. After 30 d of culturing, bioprinted constructs were stained for TUJ1, a microtubule protein present in neurons, PAX6, a marker found in cells in the neural progenitor phase, and GFAP, an intermediate filament protein expressed by astrocytes in the central nervous system [2, 15]. At day 30, TUJ1 and PAX6 were expressed in both groups (figures 6(a)–(f)). However, GFAP was only expressed in B2 constructs (figures 6(g)–(l)). Quantification of cell marker expression was also conducted for the bioprinted constructs at day 30 (figures 6(m)–(r)). TUJ1 expression was higher in B2 constructs, with 53.8 ± 5.2% of cells expressing it, against 31.5 ± 11.9% of B5 bioprinted constructs. PAX6 expression was mostly present in the B5 group, with 86.5 ± 0.2% of cells expressing it, against 46.9 ± 4.8% cells for B2 constructs. On the other hand, GFAP expression was 74.0 ± 7.4% for B2 constructs and 5.5 ± 2.5% for B5 constructs.

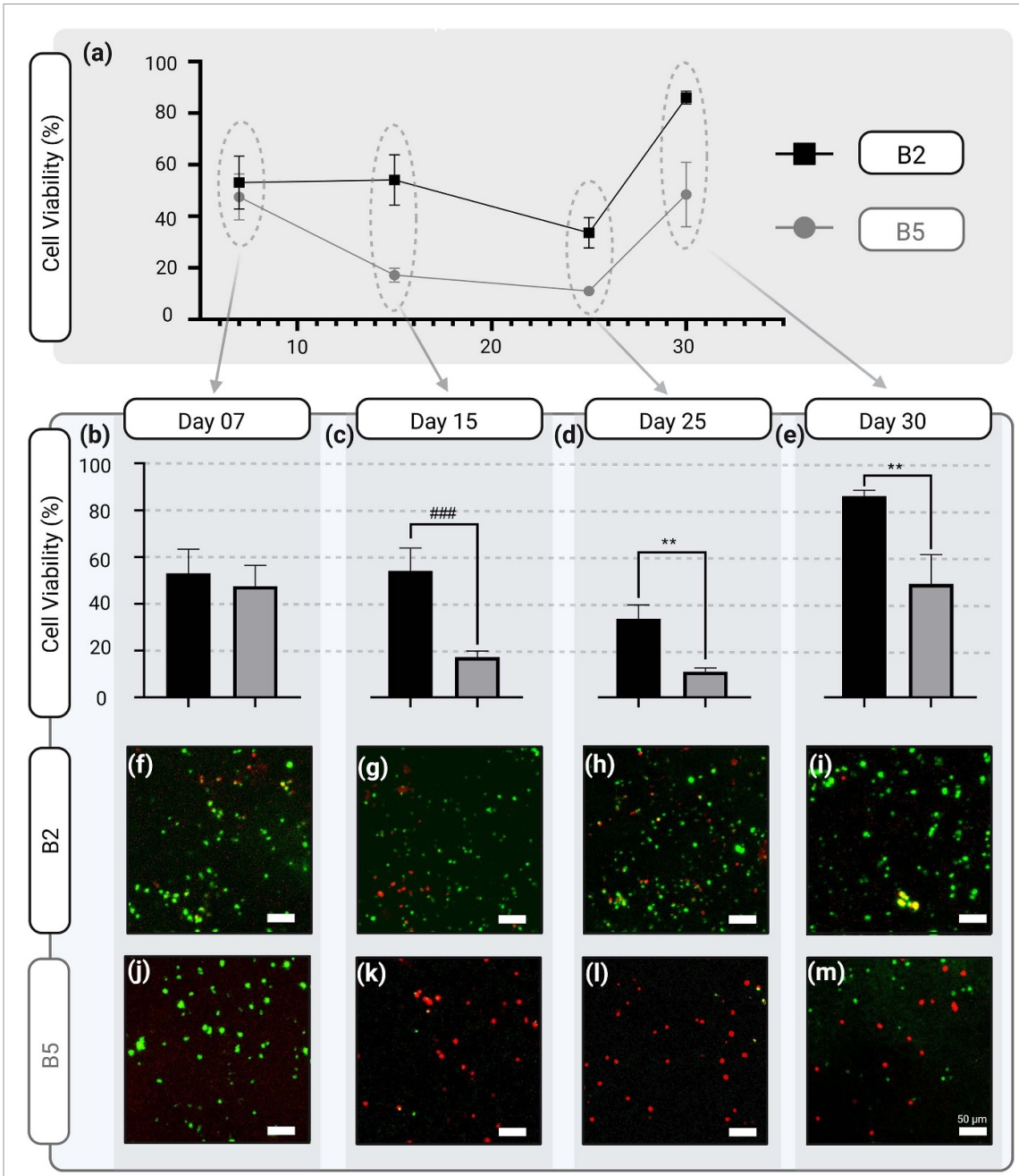

Figure 5. Cell viability of 3D bioprinted CMCS/alginate/fibrin constructs. (a) hiPSC-NPC cell viability values from live/dead assay on B2 and B5 up to 30 d of cell culture. (b)–(e) One-way ANOVA and Tukey post-hoc analysis was carried out for statistical analysis between groups at each timepoint using a confidence level of 95% ($p < 0.05$). Data reported as mean ± standard error ($n = 3$). * represents $p < 0.05$ for unpaired t-test (parametric data), ** $p < 0.01$ unpaired *t*-test (parametric data), and ### < 0.001 for Mann–Whitney (non-parametric data). hiPSC-NPC staining at specific time points after 3D bioprinting in (f)–(i)) B2 formulation and (j)–(m) B5 formulation (scale bar: 50 µm).

Statistical significance was observed only for the GFAP expression between the two bioink formulations. Additionally, an ELISA assay for the expression of brain-derived neurotrophic factor (BDNF) was performed to evaluate if B2 and B5 had any effect over this neurotrophic factor associated with hiPSC-NPC's survival and differentiation (supplemental figure S2). The ELISA assay showed that the culture media used for both hiPSC-NPC expansion and culturing 3D bioprinted constructs already had 15.71 ± 6.88 pg ml of BDNF in its composition (red line, control), which was likely consumed by the bioprinted hiPSC-NPC in the initial days of culture. Moreover, after 10 d of culture, BDNF concentration for B2 constructs increased to 24.39 ± 4.85 pg ml This suggests that the hiPSC-NPC in B2 constructs were able to express BDNF after proliferation.

hiPSC-NPCs cultured in the B2 bioink had a higher expression of both the neuron and astrocyte markers, whilst the cells cultured in the B5 bioink were mostly retained in the neural progenitor state. Given that the two groups differed only in bioink

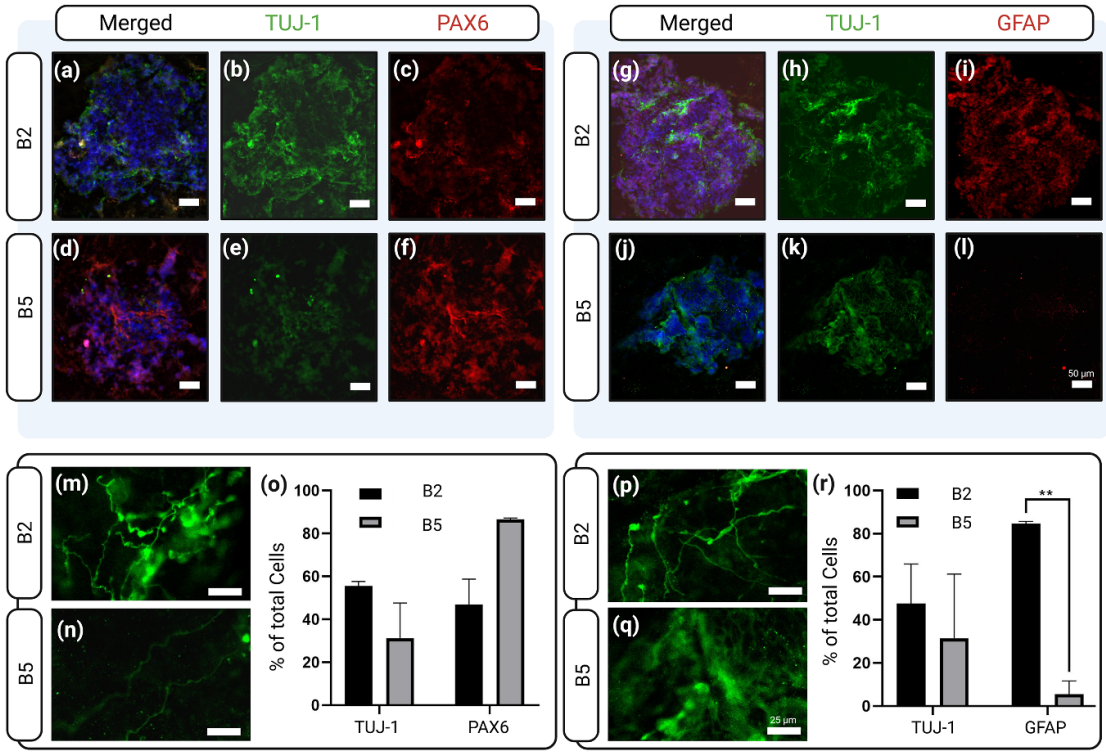

Figure 6. Immunocytochemical analysis of the 3D bioprinted constructs after 30 d of hiPSC-NPC culture. Expression of DAPI-blue, TUJ-1-green, PAX6-red and GFAP-red for cells bioprinted in (a)–(c) and (g)–(i) B2 formulation and D-F and (j)–(l)) B5 formulation. hiPSC-NPC expressed TUJ-1 and PAX6, with cell clusters interconnected by neurites after being 3D bioprinted and cultured in the (m) and (p)) B2 bioink and (n) and (q)) B5 bioink. Percentage of cells in each selected bioink formulation (B2 and B5) that expressed (o) TUJ-1 and PAX6 genes and (r)) TUJ-1 and GFAP genes.

formulation, the results suggest that the differences in the CMCS form affected cell fate. These results are consistent with previous studies that reported that chitosan promotes neuronal differentiation, as B2 constructs have residual and non-substituted amino groups [58]. However, B2 constructs also displayed significant GFAP activity, which can contribute reactive astrocytes to emerging and consequently be disadvantageous for neuroregeneration applications [59]. Nevertheless, constructs 3D bioprinted with the B2 formulation presented both neurons and astrocytes, and cell clusters were connected by neurites (figures 6(m), (n), (p) and (q)). This is an important feature because bioinks applied to 3D bioprinting of neural tissue need to support neurite growth [7]. Moreover, while the higher expression of PAX6 on B5 constructs could imply that this formulation facilitates hiPSC-NPC proliferation, this claim is not compatible with the cell viability results observed in figure 5. Therefore, it is likely that the hiPSC-NPCs cultured in the B5 constructs were retained in a neural progenitor stage with limited proliferation [47]. These results open a pathway for further investigations to describe how bioink composition, and more specifically how different compositional groups of CMCS, can affect different aspects of tissue functionality of 3D bioprinted neural tissues, such as neuron maturation, synaptogenesis, spontaneous action potentials and formation of neural networks [7].

4. Conclusion

Bioinks formulated with either N,O-CMCS or O-CMCS, alginate and fibrin at different hydrogel fractions were compared in terms of rheological and printability properties. Bioinks with low concentration of fibrin (10 mg ml^{-1}, B1 and B4) or high concentration of N,O-CMCS, O-CMCS and alginate (3% w/v, B3 and B6) lacked layer uniformity, shape fidelity and extrusion forces compatible with hiPSC-NPCs. Therefore, bioinks with 1% N,O-CMCS or O-CMCS, 1% alginate and 20 mg ml^{-1} fibrin (B2 and B5) were selected for physicochemical characterization and 3D bioprinting of neural tissues with hiPSC-NPCs. While there was no difference in the physicochemical properties of the selected bioinks, the hiPSC-NPCs in the O-CMCS based bioink (B5) suffered severe cell death and did not differentiate hiPSC-NPC into neural tissues. These results helped elucidate how the composition and physiochemical properties of a given bioink formulation can affect its biological performance regarding cell viability and differentiation into different cell types. Using a novel bioink formulated of 1% N,O-CMCS 1% alginate and 20 mg ml^{-1} fibrin (B2) we have successfully

bioprinted and differentiated hiPSC-NPC into neurons and astrocytes, therefore obtaining a 3D bioprinted construct that is able to replicate different neural cell types found in the central nervous system. The optimized bioink described in this study lays the groundwork for future works that will focus on detailing how different CMCS groups affect tissue maturation and functionality features in 3D bioprinted constructs, such as electrophysiological response and formation of neural networks, for the potential use of 3D bioprinted neural tissues for neural tissue modeling and drug screening.

Data availability statement

All data that support the findings of this study are included within the article (and any supplementary files).

ORCID iDs

Amanda C Juraski https://orcid.org/0000-0003-3998-3414
Victor A da Silva https://orcid.org/0000-0002-7062-7808
Adriano R Azzoni https://orcid.org/0000-0003-0696-4663
Stephanie M Willerth https://orcid.org/0000-0002-1665-7723

References

[1] Butler H M, Naseri E, MacDonald D S, Andrew Tasker R and Ahmadi A 2020 Optimization of starch- and chitosan-based bio-inks for 3D bioprinting of scaffolds for neural cell growth *Materialia* **12** 100737
[2] Abelseth E, Abelseth L, De La Vega L, Beyer S T, Wadsworth S J and Willerth S M 2019 3D printing of neural tissues derived from human induced pluripotent stem cells using a fibrin-based bioink *ACS Biomater. Sci. Eng.* **5** 234–43
[3] Ngo T B, Spearman B S, Hlavac N and Schmidt C E 2020 Three-dimensional bioprinted hyaluronic acid hydrogel test beds for assessing neural cell responses to competitive growth stimuli *ACS Biomater. Sci. Eng.* **6** 6819–30
[4] Murphy S V and Atala A 2014 3D bioprinting of tissues and organs *Nat. Biotechnol.* **32** 773–85
[5] Gu Q, Tomaskovic-Crook E, Lozano R, Chen Y, Kapsa R M, Zhou Q, Wallace G G and Crook J M 2016 Functional 3D neural mini-tissues from printed gel-based bioink and human neural stem cells *Adv. Healthcare Mater.* **5** 1429–38
[6] Gungor-Ozkerim P S, Inci I, Zhang Y S, Khademhosseini A and Dokmeci M R 2018 Bioinks for 3D bioprinting: an overview *Biomater. Sci.* **6** 915–46
[7] Yan Y *et al* 2024 3D bioprinting of human neural tissues with functional connectivity *Cell Stem Cell* **31** 260–274.e7
[8] Salaris F, Colosi C, Brighi C, Soloperto A, de Turris V, Benedetti M C, Ghirga S, Rosito M, Di Angelantonio S and Rosa A 2019 3D bioprinted human cortical neural constructs derived from induced pluripotent stem cells *J. Clin. Med.* **8** 1595
[9] Sahin A, Ciki B and Karademir-Yilmaz B 2023 In vitro evaluation of biomaterials for neural tissue engineering *Biomaterials for Neural Tissue Engineering* (Elsevier) pp 367–415
[10] Hwang D G, Choi Y and Jang J 2021 Bioprinting-based vascularized tissue models mimicking tissue-specific architecture and pathophysiology for in vitro Studies *Front. Bioeng. Biotechnol.* **9** 1–16
[11] Nothdurfter D, Ploner C, Coraça-Huber D C, Wilflingseder D, Müller T, Hermann M, Hagenbuchner J and Ausserlechner M J 2022 3D bioprinted, vascularized neuroblastoma tumor environment in fluidic chip devices for precision medicine drug testing *Biofabrication* **14** 035002
[12] Zhang Y, Kumar P, Lv S, Xiong D, Zhao H, Cai Z and Zhao X 2021 Recent advances in 3D bioprinting of vascularized tissues *Mater. Des.* **199** 109398
[13] Sharma R, da Silva V A, Hangad M V and Willerth S 2025 Recent developments in 3D bioprinting for neural tissue engineering *Handbook of Neural Engineering* (Elsevier) pp 549–92
[14] Wang G, Wang X and Huang L 2017 Feasibility of chitosan-alginate (Chi-Alg) hydrogel used as scaffold for neural tissue engineering: a pilot study in vitro *Biotechnol. Biotechnol. Equip.* **31** 766–73
[15] De la Vega L, Abelseth L, Sharma R, Triviño-Paredes J, Restan M and Willerth S M 2021 Bioprinting human-induced pluripotent stem cells and drug-releasing microspheres to produce responsive neural tissues *Adv. Nanobiomed. Res.* **1** 2000077
[16] Naseri E, Cartmell C, Saab M, Kerr R G and Ahmadi A 2021 Development of N,O-carboxymethyl chitosan-starch biomaterial inks for 3D printed wound dressing applications *Macromol. Biosci.* **21** 2100368
[17] Zhang X, Cheng F, Islam M R and Li H 2024 The fabrication of the chitosan-based bioink for in vitro tissue repair and regeneration: a review *Int. J. Biol. Macromol.* **257** 128504
[18] Anitha A, Divya Rani V V, Krishna R, Sreeja V, Selvamurugan N, Nair S V, Tamura H and Jayakumar R 2009 Synthesis, characterization, cytotoxicity and antibacterial studies of chitosan, O-carboxymethyl and N,O-carboxymethyl chitosan nanoparticles *Carbohydrate Polym.* **78** 672–7
[19] Xiong M, Chen Y, Hu H-J, Cheng H, Li W-X, Tang S, Hu X, Lan L-M, Zhang H and Jiang G-B 2024 Multifunctional pH-responsive hydrogel dressings based on carboxymethyl chitosan: synthesis, characterization fostering the wound healing *Carbohydrate Polym.* **341** 122348
[20] Butler H M, Naseri E, MacDonald D S, Tasker R A and Ahmadi A 2021 Investigation of rheology, printability, and biocompatibility of N,O-carboxymethyl chitosan and agarose bioinks for 3D bioprinting of neuron cells *Materialia* **18** 101169
[21] Agarwal T *et al* 2023 Chitosan and its derivatives in 3D/4D (bio) printing for tissue engineering and drug delivery applications *Int. J. Biol. Macromol.* **246** 125669
[22] Yan Y, Guan S, Wang S, Xu J and Sun C 2022 Synthesis and characterization of protocatechuic acid grafted carboxymethyl chitosan with oxidized sodium alginate hydrogel through the Schiff's base reaction *Int. J. Biol. Macromol.* **222** 2581–93
[23] Huang J, Fu H, Wang Z, Meng Q, Liu S, Wang H, Zheng X, Dai J and Zhang Z 2016 BMSCs-laden gelatin/sodium alginate/carboxymethyl chitosan hydrogel for 3D bioprinting *RSC Adv.* **6** 108423–30
[24] He Y *et al* 2021 A biodegradable antibacterial alginate/carboxymethyl chitosan/Kangfuxin sponges for promoting blood coagulation and full-thickness wound healing *Int. J. Biol. Macromol.* **167** 182–92
[25] Neufurth M, Wang S, Schröder H C, Al-Nawas B, Wang X and Müller W E G 2022 3D bioprinting of tissue units with mesenchymal stem cells, retaining their proliferative and differentiating potential, in polyphosphate-containing bio-ink *Biofabrication* **14** 015016
[26] Mohabatpour F, Duan X, Yazdanpanah Z, Tabil X L, Lobanova L, Zhu N, Papagerakis S, Chen X and Papagerakis P 2023 Bioprinting of alginate-carboxymethyl

chitosan scaffolds for enamel tissue engineering in vitro *Biofabrication* **15** 015022
[27] Zhang W, Zhong D, Liu Q, Zhang Y, Li N, Wang Q, Liu Z and Xue W 2013 Effect of chitosan and carboxymethyl chitosan on fibrinogen structure and blood coagulation *J. Biomater. Sci. Polym. Ed.* **24** 1549–63
[28] Lee C, Abelseth E, de la Vega L and Willerth S M 2019 Bioprinting a novel glioblastoma tumor model using a fibrin-based bioink for drug screening *Mater. Today Chem.* **12** 78–84
[29] Cui X, Li J, Hartanto Y, Durham M, Tang J, Zhang H, Hooper G, Lim K and Woodfield T 2020 Advances in extrusion 3D bioprinting: a focus on multicomponent hydrogel-based bioinks *Adv. Healthcare Mater.* **9** 1901648
[30] Bilkic I, Sotelo D, Anujarerat S, Ortiz N R, Alonzo M, El Khoury R, Loyola C C and Joddar B 2022 Development of an extrusion-based 3D-printing strategy for clustering of human neural progenitor cells *Heliyon* **8** e12250
[31] Tashman J W, Shiwarski D J and Feinberg A W 2021 A high performance open-source syringe extruder optimized for extrusion and retraction during FRESH 3D bioprinting *HardwareX* **9** e00170
[32] Liu W *et al* 2017 Rapid continuous multimaterial extrusion bioprinting *Adv. Mater.* **29** 1604630
[33] Jafari H, Ghaffari-bohlouli P, Podstawczyk D, Nie L and Shavandi A 2022 Tannic acid post-treatment of enzymatically crosslinked chitosan-alginate hydrogels for biomedical applications *Carbohydrate Polym.* **295** 119844
[34] Tea L, Renou F and Nicolai T 2021 Effect of hydrophobicity and molar mass on the capacity of chitosan and κ-carrageenan to stabilize water in water emulsions *Carbohydrate Polym.* **271** 118423
[35] Garrido-Maestu A, Ma Z, Paik S-Y-R, Chen N, Ko S, Tong Z and Jeong K C 2018 Engineering of chitosan-derived nanoparticles to enhance antimicrobial activity against foodborne pathogen Escherichia coli O157:H7 *Carbohydrate Polym.* **197** 623–30
[36] Tordi P, Gelli R, Ridi F and Bonini M 2024 A bioinspired and sustainable route for the preparation of Ag-crosslinked alginate fibers decorated with silver nanoparticles *Carbohydrate Polym.* **326** 121586
[37] Gorroñogoitia I, Urtaza U, Zubiarrain-Laserna A, Alonso-Varona A and Zaldua A M 2022 A study of the printability of alginate-based bioinks by 3D bioprinting for articular cartilage tissue engineering *Polymers* **14** 354
[38] Wang L and Wang A 2008 Adsorption properties of congo red from aqueous solution onto N,O-carboxymethyl-chitosan *Bioresour. Technol.* **99** 1403–8
[39] de Abreu F R and Campana-Filho S P 2009 Characteristics and properties of carboxymethylchitosan *Carbohydrate Polym.* **75** 214–21
[40] Chrenek J, Kirsch R, Scheck K and Willerth S M 2022 Protocol for printing 3D neural tissues using the BIO X equipped with a pneumatic printhead *STAR Protoc.* **3** 101348
[41] Sharma R, Kirsch R, Valente K P, Perez M R and Willerth S M 2021 Physical and mechanical characterization of fibrin-based bioprinted constructs containing drug-releasing microspheres for neural tissue engineering applications *Processes* **9** 1205
[42] De la Vega L, Karmirian K and Willerth S M 2018 Engineering neural tissue from human pluripotent stem cells using novel small molecule releasing microspheres *Adv. Biosyst.* **2** 1–11
[43] Andrade T A M, da Silva V A, Scheck K, Garay T, Sharma R and Willerth S M 2024 Bioprinting a novel skin co-culture model using human keratinocytes and fibroblasts *J. Biomed. Mater. Res. A* **113** e37831
[44] Nethercott H E, Brick D J and Schwartz P H 2011 Part IV CHARACTERIZATION: immunocytochemical analysis of human pluripotent stem cells *Human Pluripotent Stem Cells: Methods and Protocols* vol 1 P H Schwartz R L Wesselschmidt (*Methods in Molecular Biology* 767)(Humana Press)
[45] Kailasam V, Kumara B N, Prasad K S and Nirmal J 2024 Combination of self-assembling system and N,O-carboxymethyl chitosan improves ocular residence of anti-glaucoma drug *Eur. J. Pharm. Biopharm.* **197** 114208
[46] Verma M, Kumar J, Pradhan A A, Majumder N, Ghosh S and Purwar R 2024 Assessing rheological properties of oxidized Moringa oleifera gum and carboxymethyl chitosan-based self-healing hydrogel for additive manufacturing applications *Polym. Eng. Sci.* 1–10
[47] Sharma R, Smits I P M, De La Vega L, Lee C and Willerth S M 2020 Bioprinting pluripotent stem cell derived neural tissues using a novel fibrin bioink containing drug releasing microspheres *Front. Bioeng. Biotechnol.* **8** 1–12
[48] Perez M R, Sharma R, Masri N Z and Willerth S M 2021 3D Bioprinting mesenchymal stem cell-derived neural tissues using a fibrin-based bioink *Biomolecules* **11** 1250
[49] Deepthi S and Jayakumar R 2018 Alginate nanobeads interspersed fibrin network as *in situ* forming hydrogel for soft tissue engineering *Bioact. Mater.* **3** 194–200
[50] Guo H, Shen H, Ma J, Wang P, Yao Z, Zhang W, Tan X and Chi B 2023 Versatile injectable carboxymethyl chitosan hydrogel for immediate hemostasis, robust tissue adhesion barrier, and antibacterial applications *ACS Appl. Mater. Interfaces* **15** 52290–304
[51] Rosińska K, Bartniak M, Wierzbicka A, Sobczyk-Guzenda A and Bociaga D 2023 Solvent types used for the preparation of hydrogels determine their mechanical properties and influence cell viability through gelatine and calcium ions release *J. Biomed. Mater. Res. B* **111** 314–30
[52] Nashchekina Y, Militsina A, Elokhovskiy V, Ivan'kova E, Nashchekin A, Kamalov A and Yudin V 2024 Precisely printable silk fibroin/carboxymethyl cellulose/alginate bioink for 3D printing *Polymers* **16** 1027
[53] Jaikumar D, Sajesh K M, Soumya S, Nimal T R, Chennazhi K P, Nair S V and Jayakumar R 2015 Injectable alginate-O-carboxymethyl chitosan/nano fibrin composite hydrogels for adipose tissue engineering *Int. J. Biol. Macromol.* **74** 318–26
[54] Li M, Tian X, Kozinski J A, Chen X and Hwang D K 2015 Modeling mechanical cell damage in the bioprinting process employing a conical needle *J. Mech. Med. Biol.* **15** 1550073
[55] Nooranidoost M and Kumar R 2019 Geometry effects of axisymmetric flow-focusing microchannels for single cell encapsulation *Materials* **12** 2811
[56] Tricomi B J, Dias A D and Corr D T 2016 Stem cell bioprinting for applications in regenerative medicine *Ann. New York Acad. Sci.* **1383** 115–24
[57] Chen L, Xie Y, Chen X, Li H, Lu Y, Yu H and Zheng D 2024 O-carboxymethyl chitosan in biomedicine: a review *Int. J. Biol. Macromol.* **275** 133465
[58] Zhang J, Wang Y, Shu X, Deng H, Wu F and He J 2023 Magnetic chitosan hydrogel induces neuronal differentiation of neural stem cells by activating RAS-dependent signal cascade *Carbohydrate Polym.* **314** 120918
[59] Zhang Y, Chen H, Long X and Xu T 2022 Three-dimensional-engineered bioprinted in vitro human neural stem cell self-assembling culture model 3 constructs of Alzheimer's disease *Bioact. Mater.* **11** 192–205